Applied Catalysis B: Environmental 198 (2016) 133–141

Contents lists available at ScienceDirect

Applied Catalysis B: Environmental

journal homepage: www.elsevier.com/locate/apcatb

Removal of methyl mercaptan with highly-mobile silver on graphitic carbon-nitride (g-C_3N_4) photocatalyst

Taizo Sano*, Kazuhide Koike, Tomoko Hori, Tsutomu Hirakawa, Yoshihisa Ohko, Koji Takeuchi

Environmental Management Research Institute, National Institute of Advanced Industrial Science and Technology (AIST), 16-1 Onogawa, Tsukuba, Ibaraki 305-8569, Japan

ARTICLE INFO

Article history:
Received 16 March 2016
Received in revised form 17 May 2016
Accepted 22 May 2016
Available online 24 May 2016

ABSTRACT

Modification of graphitic carbon nitride (g-C_3N_4) with silver metal significantly improved the adsorption capacity and the photocatalytic degradation activity for methyl mercaptan, which is a typical sulfurous compound, under visible light. These improvements were easily obtained by the shear mixing method. The ultrafine crystallites of metallic silver were formed on surface of carbon nitride by shear mixing of HT-g-C_3N_4 (Hydrothermal treated g-C_3N_4) in aqueous solution of silver acetate. One atom of the silver captured *ca.* 0.6 molecule of methyl mercaptan on average, while a silver atom deposited on TiO_2 captured only 0.03 molecule. The migration of silver crystallites over the g-C_3N_4 surface and the formation of silver thin-layer during the adsorption of methyl mercaptan were observed by transmission electron microscopy (TEM) and X-ray photoelectron spectroscopy (XPS). The silver crystallite on g-C_3N_4 seemed to have higher mobility than that on TiO_2 to form the coordination suitable for the adsorption of methyl mercaptan. This coordination of Ag also enhanced the photocatalytic degradation of methyl mercaptan to dimethyl disulfide.

1. Introduction

Graphitic carbon nitride (g-C_3N_4) is an old and new semiconductor getting attentions recently. While g-C_3N_4 and the related compounds were discovered in 19th century [1], the significant application was rarely reported until Wang et al. revealed the photocatalytic water-splitting activity of g-C_3N_4 in 2009 [2]. After the report, g-C_3N_4 has been widely studied as a photocatalyst [3–7], a catalyst for organic synthesis [8,9], an electrode material of fuel cell or battery [10,11], a fluorescent sensor [12,13], *etc.* The reasons why g-C_3N_4 has been getting attentions were considered as follows; (1) g-C_3N_4 is composed of very common elements, C, N, and H, (2) g-C_3N_4 is semiconducting and absorbs visible light, and (3) the stability is high (*e.g.* the resistances to acid and alkalis are very high at room temperature; the thermal stability is relatively high (<500 °C in air); g-C_3N_4 is hardly dissolved with solvent), (4) g-C_3N_4 is easily synthesized by the condensation (heating) of nitrogen-rich organic compounds (*e.g.* melamine, cyanamide or dicyandiamide) at 500–650 °C [2,14]. The chemical compositions of g-C_3N_4 produced with this method are generally nonstoichiometric, and is represented as $C_3N_{4+x}H_y$ ($0<x<0.6$, $0<y<2$). The family of nonstoichiometric g-C_3N_4 is recently called as g-C_3N_4.

g-C_3N_4 can be used as a semiconducting photocatalyst for air purification working under visible light ($\lambda < 470$ nm) [15]. The band gap of g-C_3N_4 semiconductor is between 2.6–2.8 eV. Although the photocatalytic oxidation of NO or acetaldehyde with g-C_3N_4 as prepared was quite slow due to the small specific surface area (*ca.* 8 m^2/g), the NO oxidation rate was increased by 8.6 times by alkaline hydrothermal treatment at a temperature between 90–130 °C. By the treatment, the specific surface area was increased up to 64 m^2/g, and the improvement of the activity was ascribed to the increase in the surface area. If the specific surface area of g-C_3N_4 is further enlarged, the adsorption capacity and the photocatalytic activity for air pollutants would be increased. Since g-C_3N_4 has a layered structure similar to graphite, the specific surface area could be further enlarged in similar manners to the activation of graphite or other layered compounds. If g-C_3N_4 could be completely exfoliated to monolayers, the specific surface area should be increased up to 2500 m^2/g. From these considerations, it is expected that g-C_3N_4 potentially possesses the ability to capture air pollutants similarly to active carbon and to photodecompose the adsorbed pollutants under visible light.

* Corresponding author.
E-mail address: sano-t@aist.go.jp (T. Sano).

http://dx.doi.org/10.1016/j.apcatb.2016.05.057
0926-3373/

The deodorization is one of the attractive applications of photocatalyst, because the photocatalyst is suitable for the degradation of low-concentration substances with low-energy consumption and odour problems are often caused in ppb-level concentrations. The group of reduced sulfurous compounds such as hydrogen sulfide (H_2S) and methyl mercaptan (CH_3SH) are representative odour compounds emitted from raw garbage, sewage, feces, *etc*. The odour thresholds of these sulfur compounds are extremely low (*e.g.* 0.5 ppb for H_2S), and the smells are often unpleasant for human life. The guideline concentrations of H_2S and methyl mercaptan are 20 ppb and 2 ppb in Japan [16]. The photocatalytic degradation of H_2S and methyl mercaptan in gas phase by TiO_2 under UV light has been already studied [17,18], and the deposition of silver on TiO_2 efficiently improved the degradation rate of H_2S (7 times) and methyl mercaptan (14 times) [19]. The deposited silver is inferred to act as an adsorption site and as a co-catalyst that enhances the photocatalytic oxidation of the sulfur compounds.

The degradation of the sulfurous compounds with g-C_3N_4 has an advantage in indoor environments where the conventional TiO_2 photocatalyst cannot be applied because of lack of UV light, if possible. However, the modifications of g-C_3N_4 are necessary since the adsorption capacity and the degradation rate of bare g-C_3N_4 were negligible. The deposition of noble metal is a conventional method to modify surface of photocatalyst. For example, the SH functional group in sulfur compounds strongly absorbs on gold, silver, and cupper atoms [20,21]. Additionally, the deposition of metal particles possibly increases the charge separation efficiency and inhibits the recombination of electron and hole. Therefore, it is inferred that the deposition of metal species on g-C_3N_4 enhances the adsorption and the degradation of sulfur compounds as observed in the deposition of Ag on TiO_2. However, effects and deposition methods of noble metals on g-C_3N_4 are less well-investigated. The deposition of metal species on g-C_3N_4 is possible by the photodeposition and the impregnation method, which are often applied for metal-deposition on TiO_2 [22,23]. Otherwise, in our preliminary experiment, the shear mixing method, which was utilized for the delamination of graphite to graphene [24] was able to deposit several kinds of metals on g-C_3N_4.

In this paper, we prepared several kinds of metal-deposited g-C_3N_4 with three deposition methods, and analysed the adsorption capacities and the degradation activities for methyl mercaptan. Also the behaviour of silver on g-C_3N_4 were analysed for understanding the adsorption of methyl mercaptan.

2. Experimental

2.1. Preparation of Ag-deposited g-C_3N_4

g-C_3N_4 was prepared by condensation of melamine (Wako pure chemicals ind., special grade reagent) in air at 550 °C for 2 h. The chemical composition of g-C_3N_4 was analysed to be $C_3N_{4.52}H_{1.74}O_{0.17}$ by elemental analysis. The specific surface area of g-C_3N_4 was increased by the alkaline hydrothermal treatment as reported in the foregoing paper [15]. A 1.0 g portion of g-C_3N_4, 90 cm^3 of deionized water and 0.40 g of NaOH (0.11 mol/L) were mixed in a pressure tight vessel (100 cm^3) of polytetrafluoroethylene (PTFE), and the mixture was heated at 110 °C for 18 h while being stirred with a magnetic stirrer. After cooling down, the solid products was washed with 40 cm^3 of deionized water 3 times, and finally, the product was dried at 80 °C. The samples after the alkaline hydrothermal treatment was denoted as HT-g-C_3N_4.

The deposition of Ag was performed by three methods. (i) Photodeposition (PD) method: a 0.50-g portion of HT-g-C_3N_4 or g-C_3N_4 was dispersed into $AgNO_3$ aqueous solution (50 mL, 9.2×10^{-4} mol/L) in the quartz cell, and was treated with ultrasonication for 1 min. The suspension was irradiated with UV light from a high-pressure Hg lamp (Ushio, USH-500D, 500W) for 30 min while the suspension was stirred vigorously by a magnetic stirrer. The product was collected by the aid of centrifugation, and was washed with de-ionized water for 3 times. (ii) Shear mixing (SM) method: 0.20 g of HT-g-C_3N_4 and metal sources ($AgNO_3$, $AgCH_3COO$, $Fe(CH_3COO)_2$, $Cu(CH_3COO)_2{\cdot}H_2O$ and $Au(CH_3COO)_3$) were dispersed in 10 mL of water, and the suspension was mixed in a glass tube (21 mm of inner diameter) by a homogenizer with a rotor (diameter 13 mm) (AS ONE, AHG-160D) at 10000 rpm for 70 min, typically. The circumferential velocity was 6.8 m/s. The solid product was separated by a centrifugal separator and was washed with de-ionized water once. The products obtained by the PD and the SM methods were finally dried at 80 °C for 24 h (iii) Impregnation (IM) method: HT-g-C_3N_4 was mixed with a small amount of silver nitrate solution, and was dried during being ground in agate mortar. The HT-g-C_3N_4 with silver nitrate was calcined at 450 °C for 1 h, and was ground again. The prepared samples are denoted as Ag/HT-g-C_3N_4(PD, SH or IM), respectively.

The characterizations of g-C_3N_4, HT-g-C_3N_4 and metal deposited HT-g-C_3N_4 were performed with X-ray diffractometry (XRD) with Cu-Kα radiation (Rigaku, Smartlab), UV–vis diffuse reflectance spectroscopy (Shimadzu, UV-3600), transmittance electron microscopy (TEM) (Topcon, EM-002B), high angle annular dark-field scanning transmission electron microscopy (HAADF-STEM) (Tecnai, Osiris) and X-ray photoelectron spectroscopy (XPS) with Al-Kα radiation (Fisons instruments, Escalab220i-XL). The contents of Ag were analysed with X-ray fluorescence analyser (XRF) (Philips, PW2404). The specific surface areas of the solid samples were determined by BET method with N_2 adsorption at 77 K (Bel Japan Inc., BELSORP-MAX).

In XPS analysis for graphitic carbon nitride with low conductivity, neutralization by electron gun is indispensable to avoid distortion of XPS spectrum caused by 'charge up'. However, in the analysis of Ag/HT-g-C_3N_4, neutralization by electron gun was not enough and the spectrum was shifted and broadened by charge up. It is inferred that the inside of Ag/HT-g-C_3N_4 was charged up along with the surface and that the electron gun was effective only for the surface. The inside charged up could not be neutralized, and inhomogeneous charge up was possibly remained. In order to avoid the distortion of spectrum with inhomogeneous charge up, the sample was tilted at 20°, and the photoelectron emitted from surface region was mainly analysed. In this paper, the intensities and the binding energies of XPS spectra were calibrated with the highest peak of N1s (398.3 eV) since the change in the N1s spectrum was smallest among the analysed regions.

2.2. Adsorption and photocatalytic degradation of methyl mercaptan (MM)

Activities of Ag/HT-g-C_3N_4 photocatalysts were evaluated with the adsorption capacity and the photocatalytic deodorization activity of MM under visible light. These activities were analysed with the flow type reactor shown in Fig. 1. A 0.10 g portion of the photocatalyst was suspended in deionized water (1.0 cm^3) and the suspension was dispersed on a glass plate (width 50 mm and length 100 mm), followed by drying in air at 50 °C for 24 h. The glass plate with the photocatalyst was placed in a single path reactor with a borosilicate glass window. The polluted test air containing 5.0 ppm of MM was prepared by diluting the standard gas in cylinder (Takachiho chemical industrial, *ca.* 200 ppm) with purified air, and was firstly passed through the bypass tube at a flow rate of 0.50 L/min. The relative humidity was controlled to be 50% at 25 °C. After the concentration became stable, the gas line was connected to the reactor and the photocatalyst was contacted with

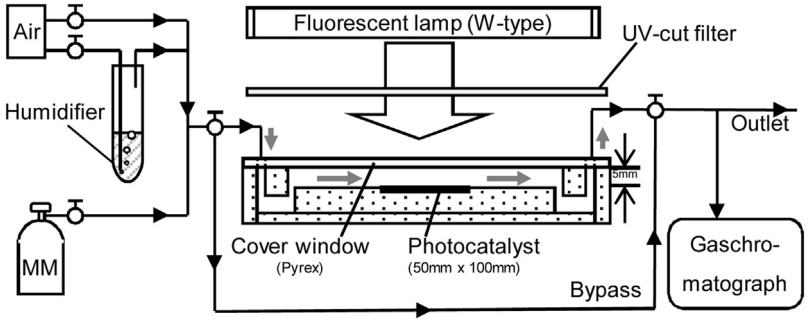

Fig. 1. Experimental setup for adsorption and photocatalytic degradation of methyl mercaptan (MM).

the test gas. The concentrations of methyl mercaptan (CH_3SH, MM) and dimethyl disulfide (CH_3SSCH_3, DMDS) eluted from the reactor or bypass tube were analysed using gaschromatograph (Shimadzu, GC-14B) with flame ionized detector (FID). Based on the decrease in the MM concentration, the amount of MM adsorbed on the sample and the adsorption capacity were calculated. After the adsorption of MM became negligible, the photocatalyst was irradiated with visible-light (6000 lx) from W-type fluorescent lamps (Toshiba, FL-10W). The most of UV light involved was removed with a long-pass filter (Nitto jushi kogyo, N-169). The cut position was 394 nm, and the transmittance below 380 nm was less than 0.3%. The number of photons with wavelength shorter than 500 nm was 3.0 mmol/h [25]. The photocatalytic degradation rate of MM was calculated from the concentrations of MM in the supply gas and effluent gas during the first 3 h of light irradiation Eq. (1).

$$\text{MM degradation rate}\,(\%) = \left(1 - \frac{[\text{effluent MM}]}{[\text{supply MM}]}\right) \times 100 \qquad (1)$$

3. Results and discussion

3.1. Adsorption and photocatalytic degradation of MM

The adsorption capacity of MM in dark and the photocatalytic degradation activity under visible light were analysed with bare g-C_3N_4, HT-g-C_3N_4, Ag/g-C_3N_4 and Ag/HT-g-C_3N_4 prepared by three kinds of Ag-deposition methods. A typical result of the adsorption and the degradation was shown in Fig. 2(a). By the contact of Ag/HT-g-C_3N_4(PD) with the polluted test air, the concentration of MM decreased steeply. Since neither other sulfur compounds, CO_2, nor CH_4 were formed, the decrease in the MM concentration were due to the adsorption of MM on Ag/HT-g-C_3N_4(PD). Once the concentration decreased to 0.5 ppm, the concentration started to increase. After 2 h, the concentration became 4.5 ppm, and the increment became small. The difference from the initial concentration (5.0 ppm) was due to the slow adsorption, which may be related to the diffusion in fine pores or relocation of MM molecules. The observation of the adsorption was stopped when the concentration exceeded 90% of the initial concentration. The amount of MM adsorbed to the photocatalyst was derived from the integral of the change in MM concentration, and the adsorption capacity per unit weight of the sample was calculated. The photocatalyst was irradiated with visible light ($\lambda > 380$ nm) following the absorption. The MM concentration decreased, and the dimethyl disulfide (DMDS) concentration increased oppositely. Formations of other gasses were not detected. The sum of the MM concentration and twice of the DMDS concentration was plotted as total S amount. The total S was only slightly smaller than the supplied MM concentration during the irradiation. These results suggest that two molecules of MM reacted to form DMDS. Although DMDS is an odour gas, the formation of DMDS from MM act as a deodorization effect since the odour threshold of DMDS is 1/2 to 1/10 of that of MM [16].

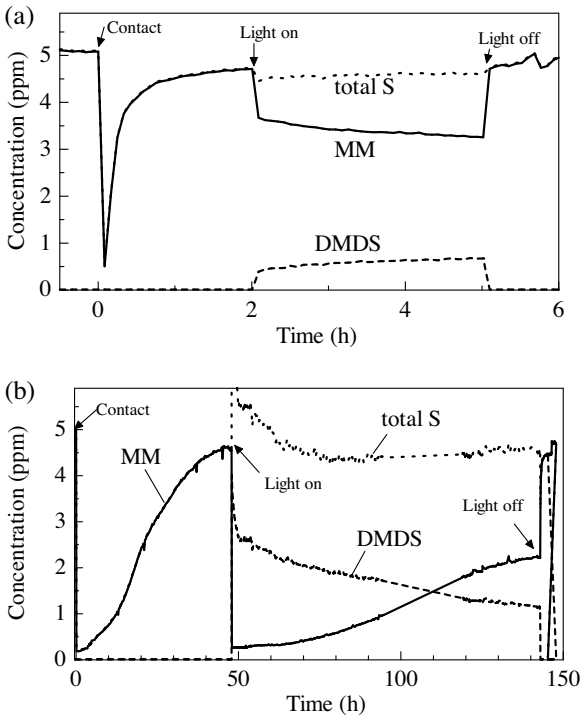

Fig. 2. Typical profile of adsorption and photocatalytic degradation of MM with Ag/HT-g-C_3N_4(PD) containing 1.0 wt% of Ag (a) and Ag/HT-g-C_3N_4(SM) with 25 wt% of Ag (b).

The adsorption capacities and the degradation rates of the prepared samples (Ag 1.0 wt%) are listed in Table 1 along with the specific surface areas of the samples and the loaded Ag. The specific surface areas of Ag were calculated by assuming that one molecule of MM adsorbed occupies 0.224 nm^2 of metal surface [26]. The bare g-C_3N_4 and HT-g-C_3N_4 without Ag adsorbed only negligible amounts of MM regardless of specific surface area. The addition of 1.0 wt% of Ag significantly changed the adsorption capacity for MM. The highest adsorption capacity was obtained when Ag was deposited to HT-g-C_3N_4 by PD method. Ag/HT-g-CN used in the experiment contained 93 μmol of Ag per g of sample, and adsorbed 21 μmol of MM per g of sample. These values indicate that one Ag atom on the carbon nitride adsorbed 0.23 molecule of MM on average. For the g-C_3N_4 without hydrothermal treatment, the IM method was more effective on the improvement of MM adsorption than the PD method, while, for HT-g-C_3N_4 with higher specific surface area, the PD method was more effective. It is inferred that silver was not well dispersed as small particles when the PD method was applied for the g-C_3N_4 with a smaller specific surface area. The

Table 1
Adsorption capacity and Photocatalytic degradation rate for MM of the photocatalysts prepared by impregnation (IM) and photodeposition (PD) methods. $AgNO_3$ was used as Ag source, and the additive amount of Ag was *ca.* 1.0 wt% to g-C_3N_4 or HT-g-C_3N_4.

Photocatalyst	Ag-deposition method	Specific surface area of sample (m^2/g)	Adsorption capacity (μmol/g)	Specific surface area of Ag (m^2/g)	Average photocatalytic degradation rate (%)
g-C_3N_4	–	7.7	0.10	–	1.0
HT-g-C_3N_4	–	48	0.20	–	2.4
Ag/g-C_3N_4	IM	10	3.3	45	7.3
Ag/HT-g-C_3N_4	IM	64	2.5	34	25
Ag/g-C_3N_4	PD	7.0	1.3	18	21
Ag/HT-g-C_3N_4	PD	48	21	283	49

specific surface areas of g-C_3N_4 and HT-g-C_3N_4 were not changed by PD method, whereas they were increased by the IM method. The surface of g-C_3N_4 or HT-g-C_3N_4 was probably etched by silver nitrate during the heat-treatment at 450 °C in the IM method to form a slightly rough surface.

The photocatalytic MM-degradation rate of Ag/HT-g-C_3N_4(PD) was 49% on average, and was highest among those of photocatalysts tested similarly to the adsorption capacity (Table 1). The degradation rates of bare g-C_3N_4 and HT-g-C_3N_4 were only 1.0% and 2.4%, respectively. The Ag deposition by PD method improved the degradation rate more effectively than that by IM method. The photocatalyst with the larger specific surface area and the higher adsorption capacity roughly possessed the higher photocatalytic degradation rate of MM, although the reason why the degradation rate by Ag/g-C_3N_4(IM) was low in spite of the relatively high adsorption capacity and why the degradation rate by Ag/g-C_3N_4(PD) was high in spite of the low adsorption capacity has not been understood yet.

In order to improve the adsorption capacity of HT-g-C_3N_4, the additive amount of Ag was increased to *ca.* 26 wt% (2.4 mmol of Ag per g of sample). Ag/HT-g-C_3N_4 prepared by the PD method with $AgNO_3$ adsorbed 340 μmol of MM per g of sample (Table 2). The value was 16 times of MM adsorbed on 1 wt% of Ag, and the average number of MM molecule adsorbed on one Ag atom was decreased to 0.14. It is suggested that the increase of additive amount of Ag in the PD method enlarged the particle size of Ag and also decreased the specific surface area by blocking the pore of HT-g-C_3N_4. Meanwhile, the adsorption capacity prepared by the SM method was 3 times or much higher than that by the PD method. Especially, when $AgCH_3COO$ was used as metal source, the obtained photocatalyst adsorbed up to 1430 μmol/g of MM, which corresponded that one atom of Ag adsorbed 0.60 molecule of MM on average. The profile of absorption of MM by Ag/HT-g-C_3N_4(SM) was shown in Fig. 2(b). The duration of adsorption was 2 days by passing test gas with 5 ppm of MM. In the case of Ag/TiO_2 prepared with typical TiO_2 (Degssa, P25) and $AgCH_3COO$ by PD method, the adsorption capacity was 79 μmol/g, and the duration was only 3 h. One atom of Ag on TiO_2 adsorbed only 0.04 molecule of MM. These results suggest that the Ag particle deposited on HT-g-C_3N_4 by SM method with $AgCH_3COO$ has the unique characteristics in the adsorption of MM.

For Ag/HT-g-C_3N_4 (SM), the specific surface area of Ag was calculated to be 787 m^2/g, and the average particle size of Ag would be 0.7 nm. The particle size was reasonable, while the specific surface area of Ag was abnormal, since it is much larger than the BET surface area of 51 m^2/g. It is speculated that (i) the MM molecule on Ag were multi-layered or (ii) the morphology of Ag particle on HT-g-C_3N_4 changed in the MM adsorption.

The photocatalytic degradation activity for MM was also improved by increasing the additive amount of Ag (Table 2). The Ag deposition by the SM method improved the activity more efficiently than by the PD method. The degradation rate of Ag/HT-g-C_3N_4(SM), which was prepared with $AgCH_3COO$ as a metal source, was highest (93% during the first 3 h of irradiation) (Fig. 2(b)). The high degradation rate was maintained for 1 day, and then was gradually decreased to 55% in the 4 days of irradiation. The decrease in the MM degradation activity was less likely to be caused by the deactivation of HT-g-C_3N_4 since the deactivation of HT-g-C_3N_4 was reported to be slower [15]. It is speculated that accumulation of SO_4^{2-} ion or change in the condition of Ag is responsible for the decrease in the performance. The further analysis of the stability of the photocatalyst is a future subject.

The formation of DMDS was observed during the light irradiation, and the decrease in the total S amount in the gas phase was less than 7%. Therefore, the predominant reaction was the photocatalytic formation of DMDS from two molecules of MM, and the small part of MM was oxidized into SO_4^{2-} and CO_2 as well as the degradation with Ag/TiO_2 under UV irradiation [19]. It is deduced that the oxidation potential of active species formed by Ag/HT-g-C_3N_4 under visible light is enough to break the S-H bond of MM but not enough to break the C-S bond. The photoinduced electron and hole Eq. (2) in graphitic carbon nitride should be involved in the MM degradation to DMDS since DMDS was produced only when the light was irradiated. It is inferred that photoinduced hole (h^+) on the carbon nitride possibly accepts the electron of thiol group of MM adsorbed Eq. (3), which is electron-donating, to form $CH_3SH_{ads.}^+$. Finally, DMDS and H_2O were formed from two molecules of $CH_3SH_{ads.}^+$ by the aid of O_2 and photoinduced electrons Eq. (4). However, the reaction mechanism has not been

Table 2
Adsorption capacity and photocatalytic degradation rate for MM of metal/HT-g-C_3N_4 prepared by shear mixing method (SM) or photodeposition method (PD).

Metal source	Deposition method	Additive amount of metal (wt%)	Specific surface area of sample (m^2/g)	Adsorption capacity (μmol/g)	Specific surface area of metal (m^2/g)	Average photocatalytic degradation rate (%)
None	–	0	48	0.20	–	2.4
$AgNO_3$	PD	27	36	340	167	76
$AgCH_3COO$	PD	25	26	310	171	31
$AgNO_3$	SM	26	37	970	496	85
$AgCH_3COO$	SM	25	51	1430	787	93
$Au(CH_3COO)_3$	SM	26	46	130	70	83[a]
$Cu(CH_3COO)_2$	SM	16	45	340	148	78
$Fe(CH_3COO)_3$	SM	14	57	0	–	4.2
$AgCH_3COO$ /TiO_2	PD	24	50	79	44	55

[a] The value involves the dark reaction from MM to DMDS.

clarified yet along with the missing hydrogen atoms of thiol groups and the participation of oxygen and/or water.

$$h\nu \rightarrow h^+ + e^- \quad (2)$$

$$CH_3SH_{ads.} + h^+ \rightarrow CH_3SH_{ads.}{}^+ \quad (3)$$

$$2CH_3SH_{ads.}{}^+ + 1/2O_2 + 2e^- \rightarrow CH_3SSCH_3 + H_2O \quad (4)$$

In the degradation for 100 h, 5.0 mmol/g of MM was changed to DMDS. Assuming that the adsorption capacity (1.43 mmol/g) is equal to the number of active site, the turn over number was 3.5. Therefore, the above reactions were photocatalytically repeated.

The effects of deposition of Au, Cu and Fe on the adsorption and the photocatalytic degradation of MM were evaluated and shown in Table 2. The Au and the Cu deposited on HT-g-C_3N_4 by the SM method adsorbed MM and enhanced the photocatalytic degradation of MM, while the addition of Fe was ineffective. The adsorption capacities of Au/HT-g-C_3N_4 and Cu/HT-g-C_3N_4 were 136 and 340 μmol/g, respectively, which were significantly smaller than that of Ag/HT-g-C_3N_4. It is inferred that the interaction of methyl mercaptan with Ag is highest among those with Au, Ag, Cu and Fe. In summary, the SM method with $AgCH_3COO$ was most effective to improve the MM-adsorption capacity of graphitic carbon nitride in this study.

Fig. 3 shows the effect of the shear mixing rate (circumferential velocity) on the activity of Ag/HT-g-C_3N_4. The adsorption capacity was increased with increasing the velocity when the treatment time was 70 min. The treatment time was also effective on the adsorption capacity. The absorption capacity of the sample treated for 10 min with 10 m/s was lower than that for 70 min with 6.8 m/s. It is considered that the reduction of Ag^+ ion on the carbon nitride is a time-consuming reactions. The photocatalytic degradation rate was also influenced by the velocity, however, the difference was small. The supply rate of MM was insufficient for the highly active samples and the degradation rates were saturated regardless of the velocity.

The dependences of Ag content in Ag/HT-g-C_3N_4 on the adsorption capacity and the photocatalytic degradation were analysed (Fig. 4). The adsorption capacity of the sample prepared by SM method increased with increasing Ag content until 25 wt%, while the capacity of the sample prepared by PD method plateaued at the content above 10 wt%. Thus, for the adsorptive removal of MM, the SM method utilized larger amount of silver than the PD method. For the photocatalytic degradation of MM, the PD method exhibited higher activity than the SM method when the Ag content were lower than 10 wt%. If the purpose of Ag addition is only to improve

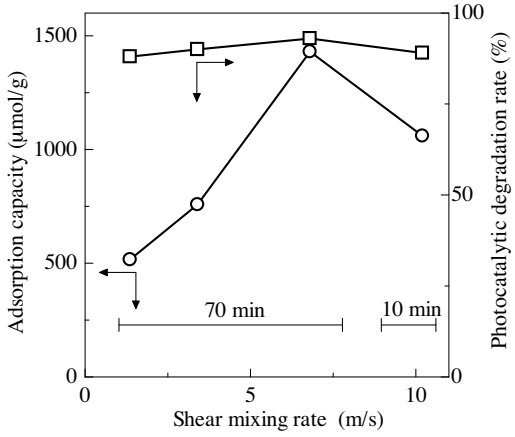

Fig. 3. Effect of shear mixing rate (circumferential velocity) on adsorption capacity (○) and photocatalytic degradation rate (□) for MM. $AgCH_3COO$ was used as metal source, and the additive amount of Ag was adjusted to *ca.* 25 wt%.

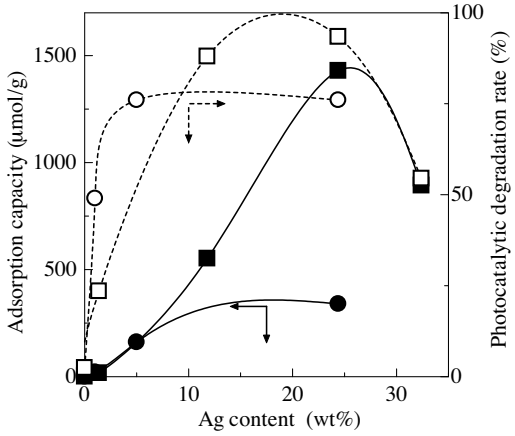

Fig. 4. Dependence of Ag contents on adsorption capacity (solid line) and photocatalytic degradation rate (dashed line) of MM. The circles (●,○) are for Ag/HT-g-C_3N_4(PD), and the squares (■, □) are for Ag-HT-g-C_3N_4(SM).

the photocatalytic degradation rate, the PD method has the advantage that the small amount of Ag effectively improves the activity. In the PD method, silver particles were possibly deposited on the photocatalytic reduction site [23] and effectively participated in the photocatalytic degradation.

3.2. Characterization of the unique Ag/HT-g-C_3N_4 prepared by shear mixing (SM) method

The characterizations of Ag/HT-g-C_3N_4(SM) prepared from $AgCH_3COO$ were performed since the phtocatalyst had revealed the unique MM-adsorption performance and the highest MM degradation activity. The XRF analysis indicated that the content of Ag was 30 ± 2 wt% when 25 wt% of Ag was mixed HT-g-C_3N_4 at the shear mixing rate of 6.8 m/s. The content percentage of Ag in the product was higher than that in the preparation suspension. This suggests that a part of HT-g-C_3N_4 was decomposed during the shear mixing. On the other hand, the Ag content was 22 ± 1 wt% when the 24 wt% of Ag was added to g-C_3N_4. The content of Ag in the product was lower than that in the preparation suspension. This indicates that a part of Ag^+ ion was remained in the aqueous phase after the shear mixing. It is considered that the efficiency of metal deposition on g-C_3N_4 with smaller surface area (7.7 m^2/g) was lower than that on HT-g-C_3N_4 with larger surface area (48 m^2/g). Generally, the Ag contents of products were between 90% and 120% of the Ag content in the preparation suspension.

The change in the crystal structure of g-C_3N_4 in the preparation of Ag/HT-g-C_3N_4 was analysed with XRD (Fig. 5). The peaks of melamine (a) were not observed in the pattern of g-C_3N_4 prepared by heating melamine at 550 °C (b). The highest peak in the pattern of g-C_3N_4 at 27.4° (d = 0.326 nm) is the diffraction peak for the stacking of carbon nitride layers [15]. The smaller diffraction peak at around 13.1 (d = 0.68 nm) was assigned to one of the structural periods in the carbon-nitride layer. The XRD pattern was not significantly changed by hydrothermal treatment in NaOH solution (c). The peaks at 27.4° and 13.1° were decreased by adding Ag (d, e). Especially, in the XRD pattern of Ag/HT-g-C_3N_4 prepared by the SM method, no diffraction peak was observed between 10 and 25 and the peak at 27.4 was considerably smaller. The decreases in the peaks indicate that the stacking of carbon nitride sheets was disordered by the shear mixing. The peak intensities were also decreased by shear mixing with $AgNO_3$, $Cu(CH_3COO)_2$ and $Fe(CH_3COO)_2$, however, were not changed with pure water. It is considered that the disordering was caused by the interaction of carbon nitride and metal species, such as insertion of Ag species

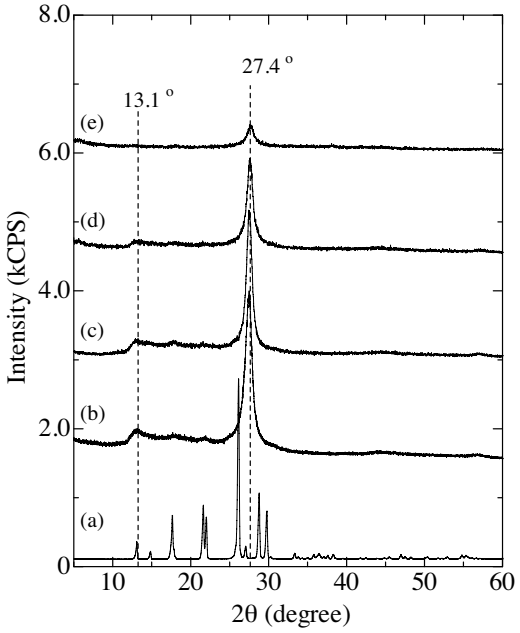

Fig. 5. XRD patterns of melamine (a), g-C_3N_4 (b), HT-g-C_3N_4 (c), and Ag/HT-g-C_3N_4 prepared by PD method (d) and SM method (e).

into interlayers of carbon nitride or coordination of Ag^+ ion to the unshared electron pair of carbon nitride. Neither peaks of metallic Ag nor Ag oxide were observed. This suggests that the Ag was deposited as ultrafine crystallites or as Ag^+ ion.

The colour of HT-g-C_3N_4 was changed to gray by deposition of silver with both of the SM method and the PD method. Although the wide range of visible light absorption from 400 nm to 800 nm was observed by UV–vis absorption spectroscopy, the absorption edge of graphitic carbon nitride at 440 nm did not shift (the spectra were not shown). It is inferred that the insertion of Ag or coordination of Ag^+ ion does not significantly change the electronic structure of graphitic carbon nitride.

Fig. 6(a)–(d) show the TEM photographs of HT-g-C_3N_4 and Ag/HT-g-C_3N_4(SM). No intelligible difference was observed between carbon nitride before Ag addition (Fig. 6 (a)) and after Ag deposition by SM method (Fig. 6(b)). Although the SM method was reported as the delamination method of graphite to graphene [24], the HT-g-C_3N_4 was not delaminated to thinner layers by the SM method even if adding several kinds of surfactants. The particle sizes of Ag on Ag/HT-g-C_3N_4 before MM adsorption were between 5 and 30 nm, and the shapes of Ag were roughly hemispherical (Fig. 6(b)). After the MM adsorption, the number of large particles decreased and the band-like Ag was observed. Additionally, the contrast of Ag to carbon nitride became smaller (Fig. 6(c)). These changes suggest that the thickness of Ag particles was decreased and Ag was 2-dimensionally spread on the surface during the MM adsorption. By the visible light irradiation, the hemispherical shape of Ag was somewhat recovered and the contrast of Ag to carbon became larger (Fig. 6(d)). These observation results suggest that the

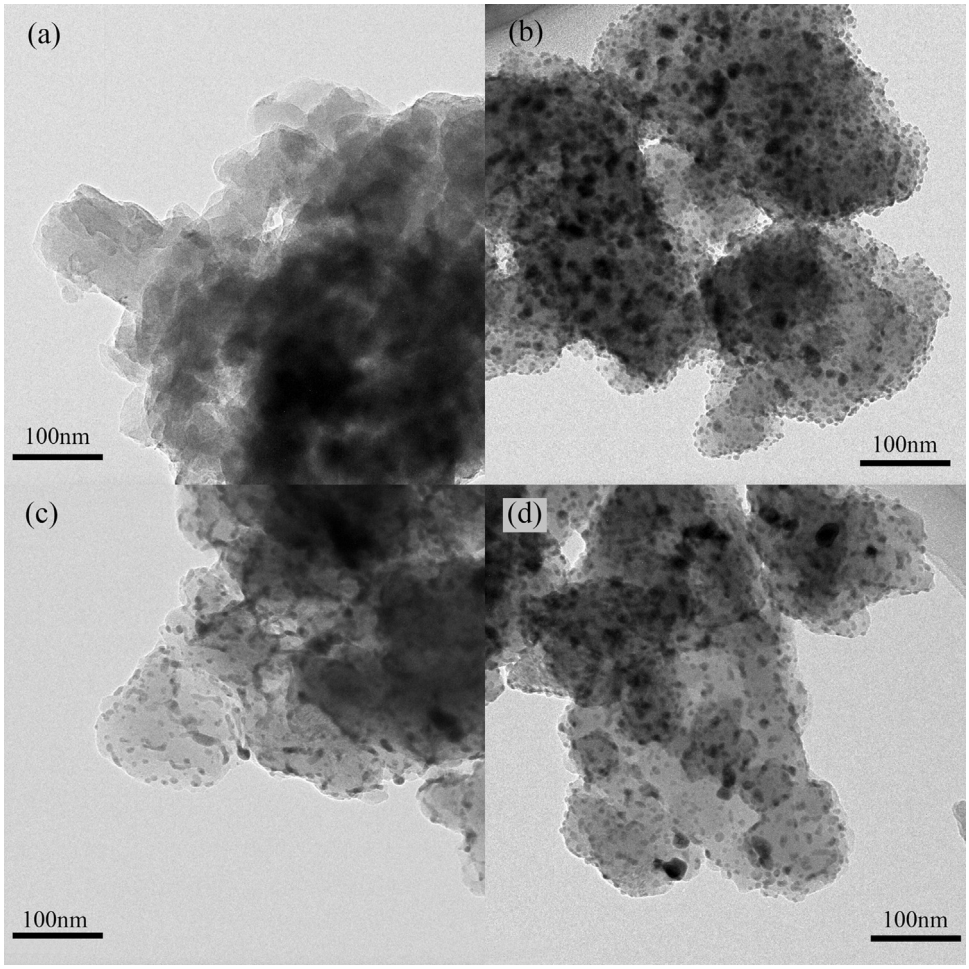

Fig. 6. TEM images of HT-g-C_3N_4 (a), Ag/HT-g-C_3N_4(SM) as prepared (b), after MM adsorption (c), and after photocatalytic deodorization under visible light (d).

Ag particle on HT-g-C_3N_4 has a flexibility that changes the morphology to adsorb a larger amount of MM. The 2-dimensionally spread Ag is considered to be favourable for MM adsorption because of the larger surface area of Ag.

However, a single crystal particle of Ag does not change the morphology in the ambient condition. Additionally, the particle size of Ag observed by TEM before MM adsorption was too large to adsorb 1430 μmol/g of MM (Table 2). For the amount of adsorption, the particle size of Ag should be smaller than 1 nm. From these considerations, the following speculation could be possible. The Ag particles were polycrystalline aggregates of smaller crystallites of Ag. The crystallites of Ag moved in order to maximize the adsorption amount of MM (Fig. 7). The driving force of the movement of Ag was the energetic stabilization by the strong interaction of Ag and MM. The movement of Ag was not observed by TEM for Ag/HT-g-C_3N_4 and Ag/TiO_2 prepared by the PD method. It is plausible that the Ag crystallites formed by PD method were larger than that formed by SM method.

The distribution of elements of Ag/HT-g-C_3N_4(SM) was analysed with High Angle Annular Dark-Field Scanning Transmission Electron Microscopy (HAADF-STEM) (Fig. 8). In a HAADF image, a heavier atom is presented as whiter. It is confirmed that the Ag atom, which was the heaviest atom contained, was distributed widely on the HT-g-C_3N_4 particle while the concentration of Ag was not homogeneous. The density of oxygen atom was tenuously tied to that of Ag and the content of oxygen was 15 atom% against Ag. These results support that the Ag on HT-g-C_3N_4 was mainly in the state of metallic Ag, which had been formed by the reduction of $AgCH_3COO$ with the terminals of carbon nitride in the shear mixing. Since the distribution of oxygen was similar to those of carbon and nitrogen, the oxygen in the Ag/HT-g-C_3N_4 was probably due to the hydrolysis of carbon nitride.

The surface of Ag/HT-g-C_3N_4(SM) was analysed by XPS (Fig. 9(a)–(d)). The change in the morphology of Ag along with the MM adsorption was supported. The binding energy of Ag3d was 367.7 eV, which was attributed to metallic Ag. The integrated area of Ag3d peak was increased with MM adsorption. This result indicates that the content of Ag atom existing near the outer surface was increased in the MM adsorption. The increase of the Ag on the outer surface was attributed to the change in the morphology from hemispherical Ag particles to the 2-dimensionally spread Ag, which had been observed by TEM. The peak intensity of Ag was decreased with photo-irradiation while the peak intensity was not completely recovered.

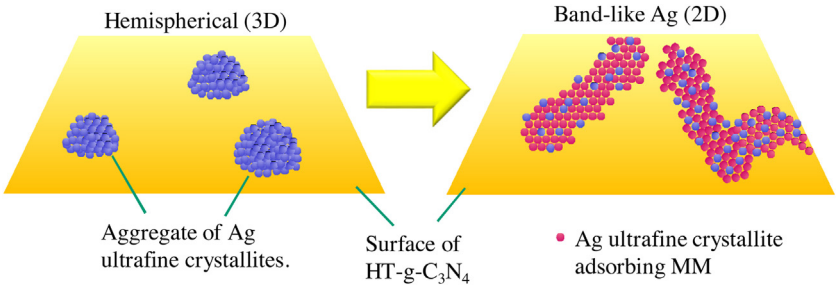

Fig. 7. Schematic model of migration of Ag ultrafine crystallites on HT-g-C_3N_4 in MM adsorption.

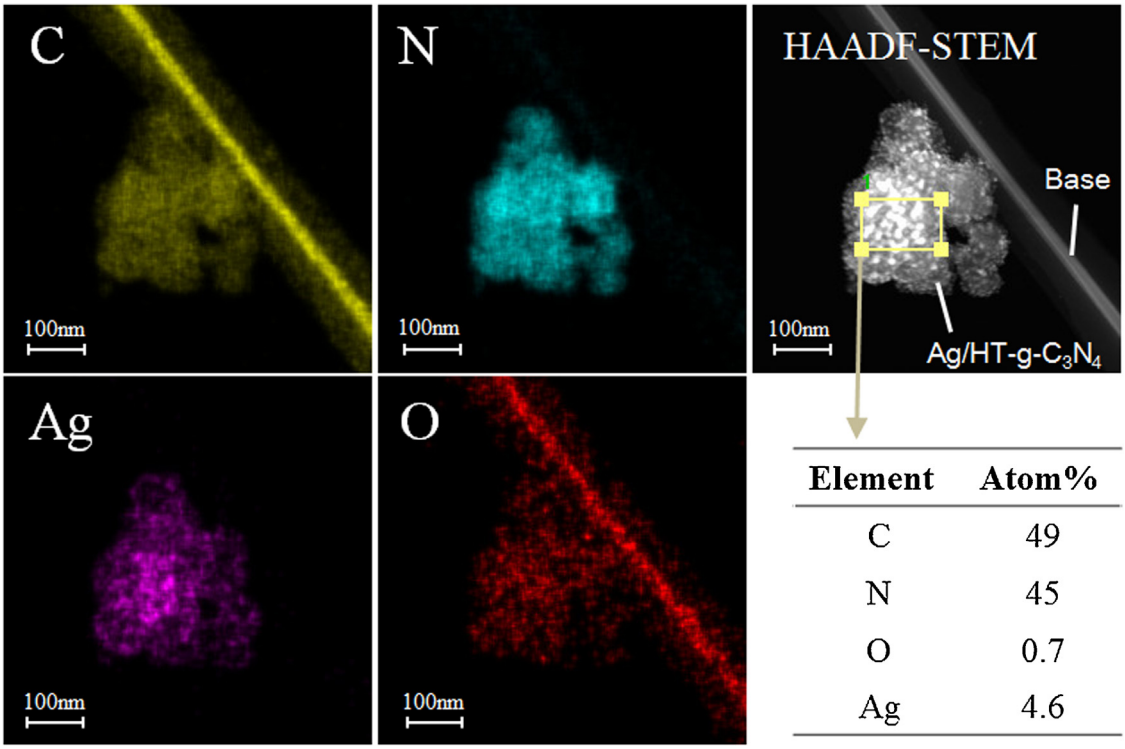

Element	Atom%
C	49
N	45
O	0.7
Ag	4.6

Fig. 8. HAADF-STEM images of Ag/HT-g-C_3N_4 (SM) with 25 wt% of Ag.

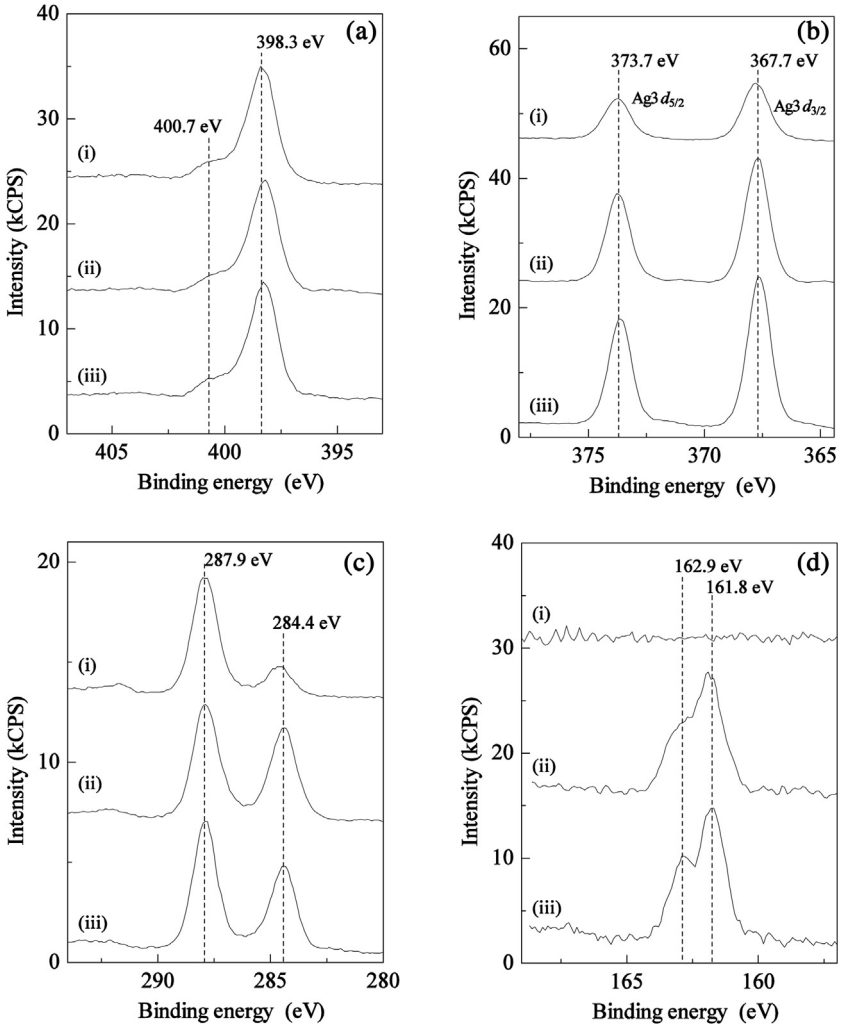

Fig. 9. X-ray photoelectron spectra (XPS) of Ag/HT-g-C_3N_4(SM) for N1s (a), Ag1s (b), C1s (c) and S1s (d). (i) as prepared, (ii) after adsorption of MM, (iii) after visible light irradiation.

The peak of C1s at 284.4 eV and the peak of S1s at 161.8 eV (and 162.9 eV) increased with the MM adsorption. These peaks were attributed to the carbon atom of methyl group and the sulfur atom of thiol group of the adsorbed MM, respectively. These peaks became slightly smaller in the photo-irradiation, however, did not return to the peak intensity before the MM adsorption. It is inferred that the photo-irradiation induces the degradation of adsorbed MM, however, a major part of MM remained on the Ag to avoid recovering the morphology of Ag to the hemispherical shape. This is also consistent with the observation with TEM. The formation of SO_4^{2-} (167–170 eV [19,27]) was not confirmed. The spectrum of O1s region was not significantly changed by the adsorption and the degradation. It is inferred that the oxygen atom contained in Ag/HT-g-C_3N_4 has a minor function in the MM degradation.

4. Conclusions

The ultrafine crystallites of metallic Ag were formed on HT-g-C_3N_4 by the reduction of $AgCH_3COO$ in the shear mixing, and contributed to the high adsorption capacity and the high photocatalytic degradation for MM. Ag/HT-g-C_3N_4 prepared by the shear mixing method with 25 wt% of Ag exhibited the highest MM adsorption capacity among the samples prepared. The average number of MM molecules adsorbed on one Ag atom was 0.60, which was significantly higher than the value for Ag/TiO_2. The Ag ultrafine crystallites moved over the surface of graphitic carbon nitride to make a coordination effective for the adsorption of MM. In the photocatalytic degradation of MM, the major reaction was the formation of a DMDS molecule from two MM molecules. The deodorization effect by the formation of DMDS is lower than that by the oxidation of MM to SO_4^{2-}, which was possible with TiO_2 and UV irradiation. However, Ag/HT-g-C_3N_4 has an advantage that visible light is utilized for the activation. Additionally, there is a possibility that an enlargement of the surface area of g-C_3N_4 will further improve the adsorption capacity and the degradation activity. The utilization of Ag ultrafine crystallites with high mobility for other reactions is also the subject of future investigation.

Acknowledgement

The authors thank Dr. Yoshizawa and Dr. Takatsuki for operating the TEM, and thank to Dr. Ohki and Dr. Noguchi for XRF analysis. This work is supported by JSPS KAKENHI 23760679.

References

[1] J. Liebig, Uber einige Stickstoff – Verbindungen, Annalen der Pharmacie 10 (1834) 1–47.
[2] X.C. Wang, K. Maeda, A. Thomas, K. Takanabe, G. Xin, J.M. Carlsson, K. Domen, M. Antonietti, A metal-free polymeric photocatalyst for hydrogen production from water under visible light, Nat. Mater. 8 (2009) 76–80.

[3] H. Wang, W.Y. Zhang, R. Tang, R.P. Hebbel, M.A. Kowalska, C.X. Zhang, J.D. Marth, M. Fukuda, C.H. Zhu, Y.Q. Huo, Core2 1–6-N-Glucosaminyltransferase-I deficiency protects injured arteries from neointima formation in apoE-Deficient mice, Arteriosclerosis Thrombosis Vascular Biol. 29 (2009) 1053–U1125.
[4] Y.J. Zhang, T. Mori, J.H. Ye, Polymeric carbon nitrides: semiconducting properties and emerging applications in photocatalysis and photoelectrochemical energy conversion, Sci. Adv. Mater. 4 (2012) 282–291.
[5] P.D. Tran, L.H. Wong, J. Barber, J.S.C. Loo, Recent advances in hybrid photocatalysts for solar fuel production, Energy Environ. Sci. 5 (2012) 5902–5918.
[6] Y. Wang, X.C. Wang, M. Antonietti, Polymeric graphitic carbon nitride as a heterogeneous organocatalyst: from photochemistry to multipurpose catalysis to sustainable chemistry, Angew. Chem. Int. Ed. 51 (2012) 68–89.
[7] Z.Y. Jin, Q.T. Zhang, S.S. Yuan, T. Ohno, Synthesis high specific surface area nanotube g-C_3N_4 with two-step condensation treatment of melamine to enhance photocatalysis properties, RSC Adv. 5 (2015) 4026–4029.
[8] A. Thomas, A. Fischer, F. Goettmann, M. Antonietti, J.O. Muller, R. Schlogl, J.M. Carlsson, Graphitic carbon nitride materials: variation of structure and morphology and their use as metal-free catalysts, J. Mater. Chem. 18 (2008) 4893–4908.
[9] X.F. Chen, J.S. Zhang, X.Z. Fu, M. Antonietti, X.C. Wang, Fe-g-C_3N_4-catalyzed oxidation of benzene to phenol using hydrogen peroxide and visible light, J. Am. Chem. Soc. 131 (2009) 11658–11659.
[10] Y. Zheng, J. Liu, J. Liang, M. Jaroniec, S.Z. Qiao, Graphitic carbon nitride materials: controllable synthesis and applications in fuel cells and photocatalysis, Energy Environ. Sci. 5 (2012) 6717–6731.
[11] S.M. Aspera, H. Kasai, H. Kawai, Density functional theory-based analysis on O_2^- molecular interaction with the tri-s-triazine-based graphitic carbon nitride, Surf. Sci. 606 (2012) 892–901.
[12] E.Z. Lee, S.U. Lee, N.S. Heo, G.D. Stucky, Y.S. Jun, W.H. Hong, A fluorescent sensor for selective detection of cyanide using mesoporous graphitic carbon(IV) nitride, Chem. Commun. 48 (2012) 3942–3944.
[13] C.M. Cheng, Y. Huang, X.Q. Tian, B.Z. Zheng, Y. Li, H.Y. Yuan, D. Xiao, S.P. Xie, M.M.F. Choi, Electrogenerated chemiluminescence behavior of graphite-like carbon nitride and its application in selective sensing Cu2+, Anal. Chem. 84 (2012) 4754–4759.
[14] T. Tyborski, C. Merschjann, S. Orthmann, F. Yang, M.C. Lux-Steiner, T. Schedel-Niedrig, Tunable optical transition in polymeric carbon nitrides synthesized via bulk thermal condensation, J. Phys.-Condens. Matter 24 (2012) 162201.
[15] T. Sano, S. Tsutsui, K. Koike, T. Hirakawa, Y. Teramoto, N. Negishi, K. Takeuchi, Activation of graphitic carbon nitride (g-C_3N_4) by alkaline hydrothermal treatment for photocatalytic NO Oxidation in gas phase, J. Mater. Chem. A (2012).
[16] Offensive odor control law, Ministry of the Environment, Government of Japan, Low No. 91 (1971).
[17] A.V. Vorontsov, E.V. Savinov, L. Davydov, P.G. Smirniotis, Photocatalytic destruction of gaseous diethyl sulfide over TiO_2, Appl. Catal. B-Environ. 32 (2001) 11–24.
[18] M.C. Canela, R.M. Alberici, W.F. Jardim, Gas-phase destruction of H2S using TiO_2/UV-VIS, J. Photochem. Photobiol. A-Chem. 112 (1998) 73–80.
[19] S. Kato, Y. Hirano, M. Iwata, T. Sano, K. Takeuchi, S. Matsuzawa, Photocatalytic degradation of gaseous sulfur compounds by silver-deposited titanium dioxide, Appl. Catal. B-Environ. 57 (2005) 109–115.
[20] M. Cohen-Atiya, D. Mandler, Studying thiol adsorption on Au, Ag and Hg surfaces by potentiometric measurements, J. Electroanal. Chem. 550 (2003) 267–276.
[21] P.E. Laibinis, G.M. Whitesides, D.L. Allara, Y.T. Tao, A.N. Parikh, R.G. Nuzzo, Comparison of the structures and wetting properties of self-assembled monolayers of normal-alkanethiols on the coinage metal-surfaces, Cu Ag, Au, J. Am. Chem. Soc. 113 (1991) 7152–7167.
[22] T. Sano, N. Negishi, K. Uchino, J. Tanaka, S. Matsuzawa, K. Takeuchi, Photocatalytic degradation of gaseous acetaldehyde on TiO_2 with photodeposited metals and metal oxides, J. Photochem. Photobiol. A-Chem. 160 (2003) 93–98.
[23] T. Sano, N. Negishi, D. Mas, K. Takeuchi, Photocatalytic decomposition of N_2O on highly dispersed Ag^+ ions on TiO_2 prepared by photodeposition, J. Catal. 194 (2000) 71–79.
[24] K.R. Paton, E. Varrla, C. Backes, R.J. Smith, U. Khan, A. O'Neill, C. Boland, M. Lotya, O.M. Istrate, P. King, T. Higgins, S. Barwich, P. May, P. Puczkarski, I. Ahmed, M. Moebius, H. Pettersson, E. Long, J. Coelho, S.E. O'Brien, E.K. McGuire, B.M. Sanchez, G.S. Duesberg, N. McEvoy, T.J. Pennycook, C. Downing, A. Crossley, V. Nicolosi, J.N. Coleman, Scalable production of large quantities of defect-free few-layer graphene by shear exfoliation in liquids, Nat. Mater. 13 (2014) 624–630.
[25] T. Sano, N. Mera, Y. Kanai, C. Nishimoto, S. Tsutsui, T. Hirakawa, N. Negishi, Origin of visible-light activity of N-doped TiO_2 photocatalyst: behaviors of N and S atoms in a wet N-doping process, Appl. Catal. B 128 (2012) 77–83.
[26] T. Miyoshi, S. Tanada, K. Boki, Properties of 13 kinds of adsorbents for removal of hydrogen-Sulfide, methanethiol, methyl sulfide, trimethylamine, and ammonia, Jpn. J. Ind. Health 19 (1977) 2–7.
[27] C.D. Wangner, Practical Surface Analysis, 2nd ed., Wiley, New York, 1990.